Research Article

Zorgati Anis*, Gallala Wissem, Vakhshoori Vali, Habib Smida, and Gaied Mohamed Essghaier

GIS-based landslide susceptibility mapping using bivariate statistical methods in North-western Tunisia

https://doi.org/10.1515/geo-2019-0056
Received Apr 25, 2019; accepted Sep 12, 2019

Abstract: The Tunisian North-western region, especially Tabarka and Ain-Drahim villages, presents many landslides every year. Therefore, the landslide susceptibility mapping is essential to frame zones with high landslide susceptibility, to avoid loss of lives and properties. In this study, two bivariate statistical models: the evidential belief functions (EBF) and the weight of evidence (WoE), were used to produce landslide susceptibility maps for the study area. For this, a landslide inventory map was mapped using aerial photo, satellite image and extensive field survey. A total of 451 landslides were randomly separated into two datasets: 316 landslides (70%) for modelling and 135 landslides (30%) for validation. Then, 11 landslide conditioning factors: elevation, slope, aspect, lithology, rainfall, normalized difference vegetation index (NDVI), land cover/use, plan curvature, profile curvature, distance to faults and distance to drainage networks, were considered for modelling. The EBF and WoE models were well validated using the Area Under the Receiver Operating Characteristic (AUROC) curve with a success rate of 87.9% and 89.5%, respectively, and a predictive rate of 84.8% and 86.5%, respectively. The landslide susceptibility maps were very similar by the two models, but the WoE model is more efficient and it can be useful in future planning for the current study area.

Keywords: Landslide susceptibility mapping, bivariate statistical model, Tunisia, weight of evidence, evidential belief functions

***Corresponding Author: Zorgati Anis:** Universite de Gabes Institut Superieur des Sciences et Techniques des Eaux Gabes Sousse, Sousse, Tunisia; Email: zorgati.aniss@gmail.com
Gallala Wissem, Vakhshoori Vali, Gaied Mohamed Essghaier: Universite de Gabes Institut Superieur des Sciences et Techniques des Eaux Gabes Sousse, Sousse, Tunisia
Habib Smida: Faculty of Earth Sciences, King Abdulaziz University, Jeddah Saudi Arabia; Laboratory of Water Energy and Envirenment, University of Sfax Tunisia; Email: habib.smida@fsg.rnu.tn

1 Introduction

Landslides are considered among the most dangerous natural hazards due to their effect on human's lives and properties [1, 2]. The north western area of Tunisia presents many landslides every year. For example in February 2012, Ain-Drahim village was isolated due to roads destruction by landslides. In addition, 98 people were directly affected and 7 deaths were reported according to National Database of Disaster Losses [3]. Despite the importance of landslide study and zonation in the Tunisian North western area, there are no studies done in the region.

Landslides are controlled by several natural conditioning factors such as: slope, rainfall, lithology, tectonics, etc. [2, 4]. So, in nature there are areas which are more prone to landslides than others whereby landslide susceptibility is defined as the spatial distribution or probability of the occurrence of landslides [5–7]. The damage of landslides could be significantly decreased by establishing landslide susceptibility maps [8].

The assessment of slope stability is carried out using two approaches [9–11]: the direct or qualitative method based on expert knowledge [12] and the indirect or quantitative method based on statistical algorithms [2, 10, 13]. The direct or qualitative method such as analytical hierarchy process (AHP) was used in landslide susceptibility mapping [14–16]. The indirect or quantitative method was widely used in the literature as the artificial neural network (ANN) [17–19], support vector machine (SVM) [20, 21] and neuro-fuzzy [22, 23]. Also the bivariate statistical methods as an indirect methods were used by many researchers like the certainty factor (CF) [6, 24, 25], statistical index (SI) [6, 26, 27], frequency ratio (FR) [8, 28, 29], evidential belief function (EBF) [30–32], weight of evidence (WoE) [6, 26, 33]. Also, the multivariate method as the logistic regression was applied in several works [34–36].

The landslide susceptibility mapping statistical methods were widely compared in the literature in different geological, climatologic, geomorphologic, etc. conditions [6, 32, 37] and results show that practically all methods were

similar with high accuracy. For example, Pradhan and Lee [38] reported that the ANN, FR and LR methods were very similar in landslide susceptibility mapping. Also, Park [39] noticed an insignificant difference in the landslide susceptibility maps (LSMs) produced using FR, AHP, ANN and LR methods.

The main aim of this study is the establishment of landslide susceptibility maps of the current study area using two bivariate statistical methods: the evidential belief function (EBF) and weight of evidence (WoE).

2 Study area

The study area covering 860 km^2, is located in the North-West of Tunisia, between Ain-Drahim and Tabarka villages, which extends from longitude 8° 25' 29" E to 8° 59' 53" E and from latitude 36° 40' 26" N to 37° 00' 36" N (Figure 1). This zone is situated at an altitude ranging between 3 and 1000m above msl in a mountainous area. The lithological units of the area are mainly composed by the Numidian flyschoidal deposits of Oligocene, lower-Miocene age, essentially consisting of turbiditic sandy and clayey formation [40–44]. The flysch formations present large changes in structural style [45] and are heterogeneous rock masses which lead to the alteration of hard rock layers (sandstone and siltstones) and weak ones (marls and clay). Also, flysch rocks are influenced by weathering processes which cause changes in strength properties and increases the content of the clay fraction in the weathered zone by alteration of silicate minerals in clay, silt, sand and sandstone [46] which make flysch rocks more prone to landslide.

The climate of the study area is considered Mediterranean, with rainy winters and warm summers. The precipitation ranges from 630 mm (1993) to 2400 mm (2003) with a yearly average precipitation above 1000mm according to the National Institute of Meteorology [47].

3 Data preparation

3.1 Landslide inventory map

A landslide inventory map is crucial for landslide susceptibility mapping [48, 49]. This map is the base for the landslide occurrence probability calculation by defining the relationship between landslide occurrences and factors related to them in the past [50–52].

The landslide inventory map of the studied area was produced by aerial photo interpretation with large scale field surveys. Only rotational, transitional and compound landslides were taken into account due to their similar conditioning factors [28]. Thus, 451 landslides were identified in the study area and mapped as polygons. They were randomly subdivided into two data sets: 70% (316 landslides) for the susceptibility model building and 30% (135 landslides) for model validation (Figure 1).

3.2 Preparation of landslide conditioning factors

For this study 11 factors which are: elevation, lithology, slope angle, slope aspect, plan curvature, profile curvature, distance to drainage network, distance to fault, rainfall, NDVI and land use/cover were prepared in ARCGIS 10.4 database as landslide conditioning factors.

3.3 Elevation

Altitude is considered as a landslide factor in many research papers [53, 54]. In this study, a DEM with 30 x 30 grid size was used and reclassified into five classes with a 200m interval: <200, 200-400, 400-600, 600-800 and >800 (Figure 2b).

3.4 Slope angle

As one of most important factor of landslide susceptibility mapping, slope angle is usually used in landslide susceptibility mapping [26, 28, 51]. The slope angle of the study area ranges between 0 and 60°, it was reclassified into six classes with 10° interval: <10°, 10°-20°, 20°-30°, 30°-40°, 40°-50° and >50° (Figure 2j).

3.5 Slope aspect

Slope aspect is the direction of the slope angle and is considered as a landslide conditioning factor in several researches [55], due to numerous conditions such as weight of slope exposure to sunlight, cold and hot winds, rainfall and discontinuities [52, 56, 57]. The slope aspect is derived from DEM in ARCGIS software and reclassified into nine classes: flat (–1), north (0°-22.5°, 337.5°-360°), northeast (22.5°-67.5°), east (67.5°-112.5°), southeast (112.5°-157.5°), south (157.5°-202.5°), southwest (202.5°-

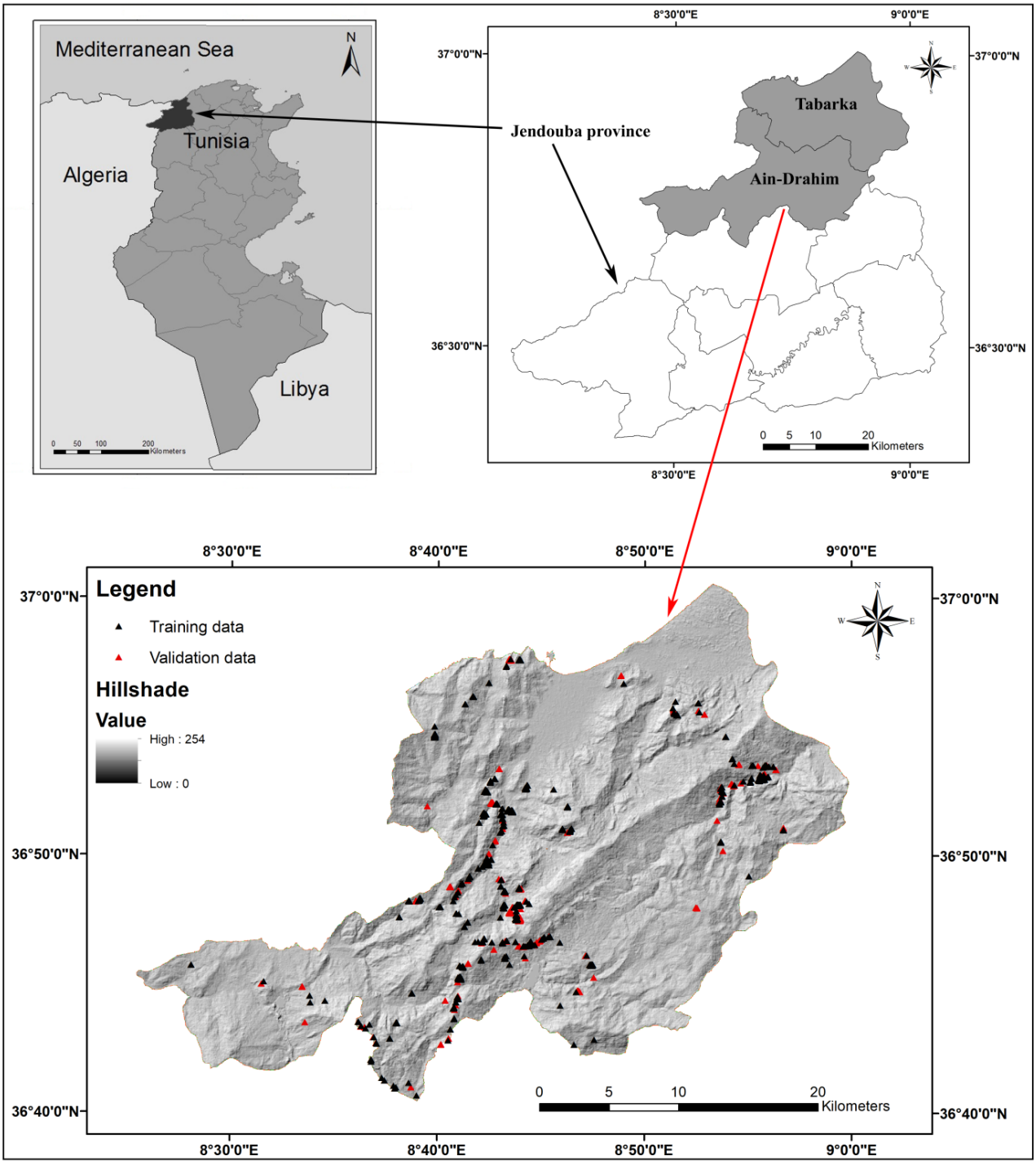

Figure 1: Study area location with landslide inventory.

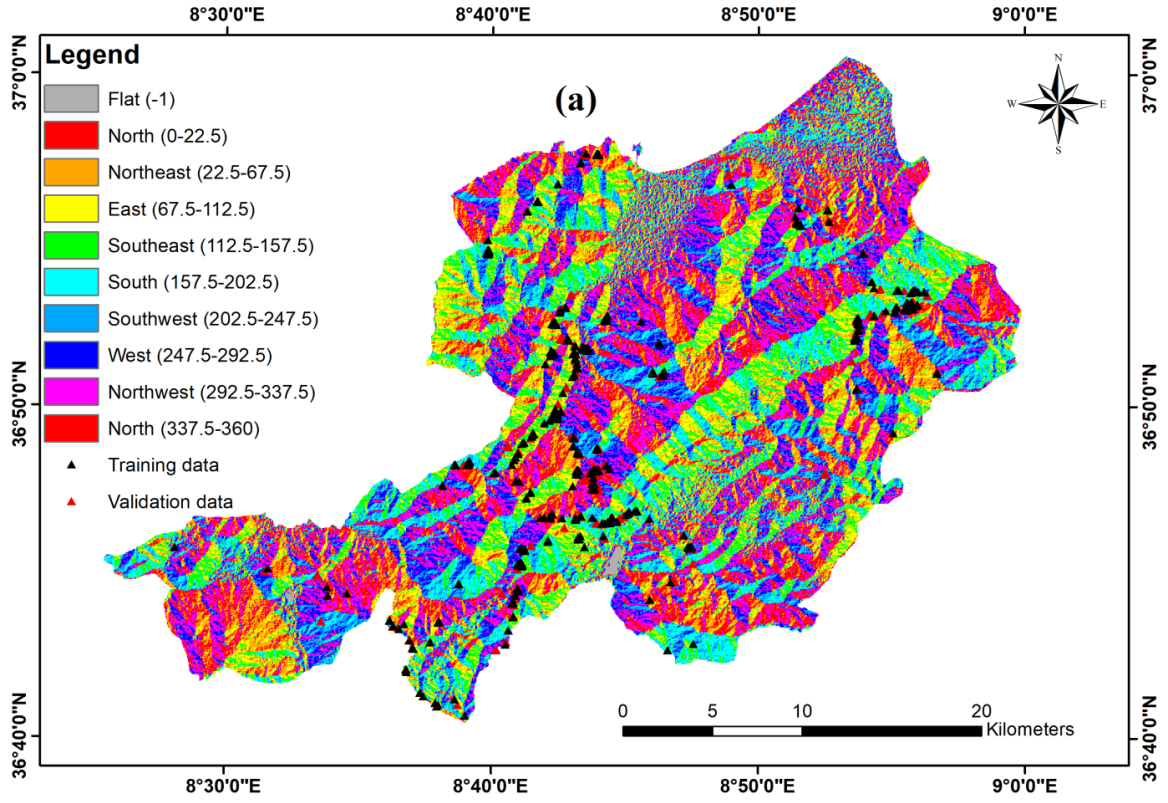

Figure 2a: Landslide conditioning factors – slope aspect

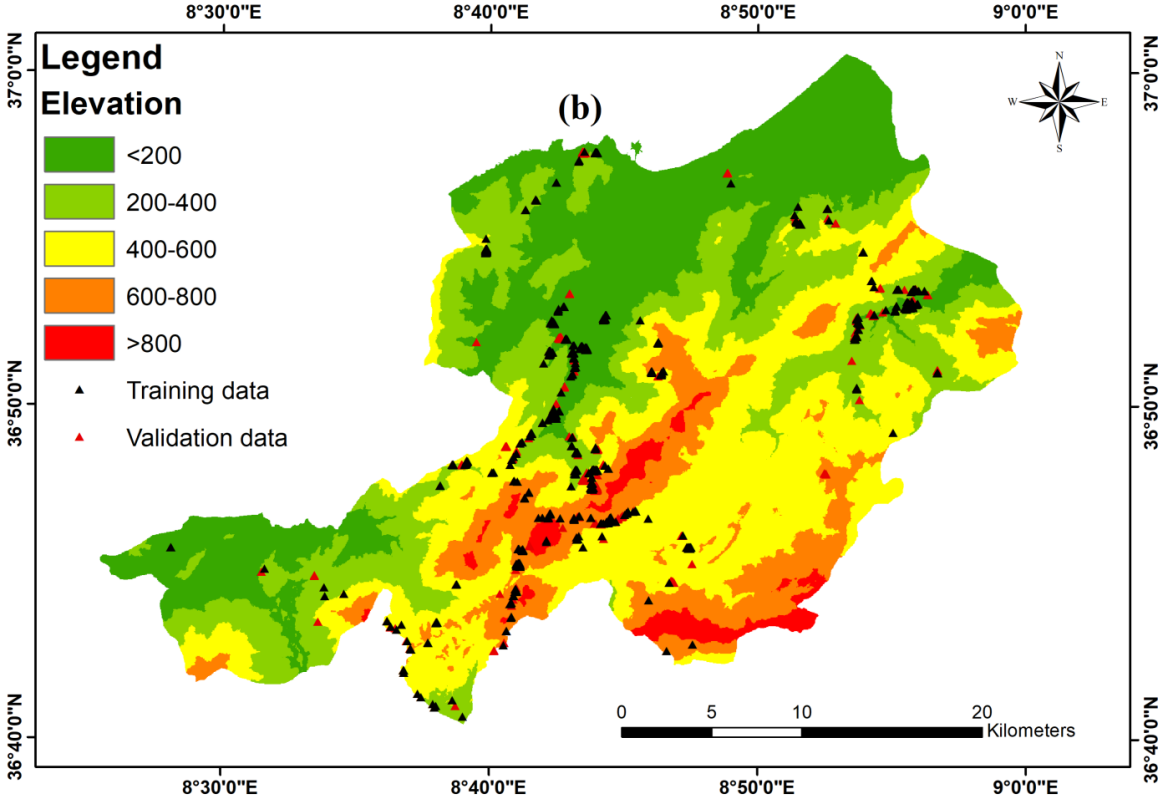

Figure 2b: Landslide conditioning factors – elevation

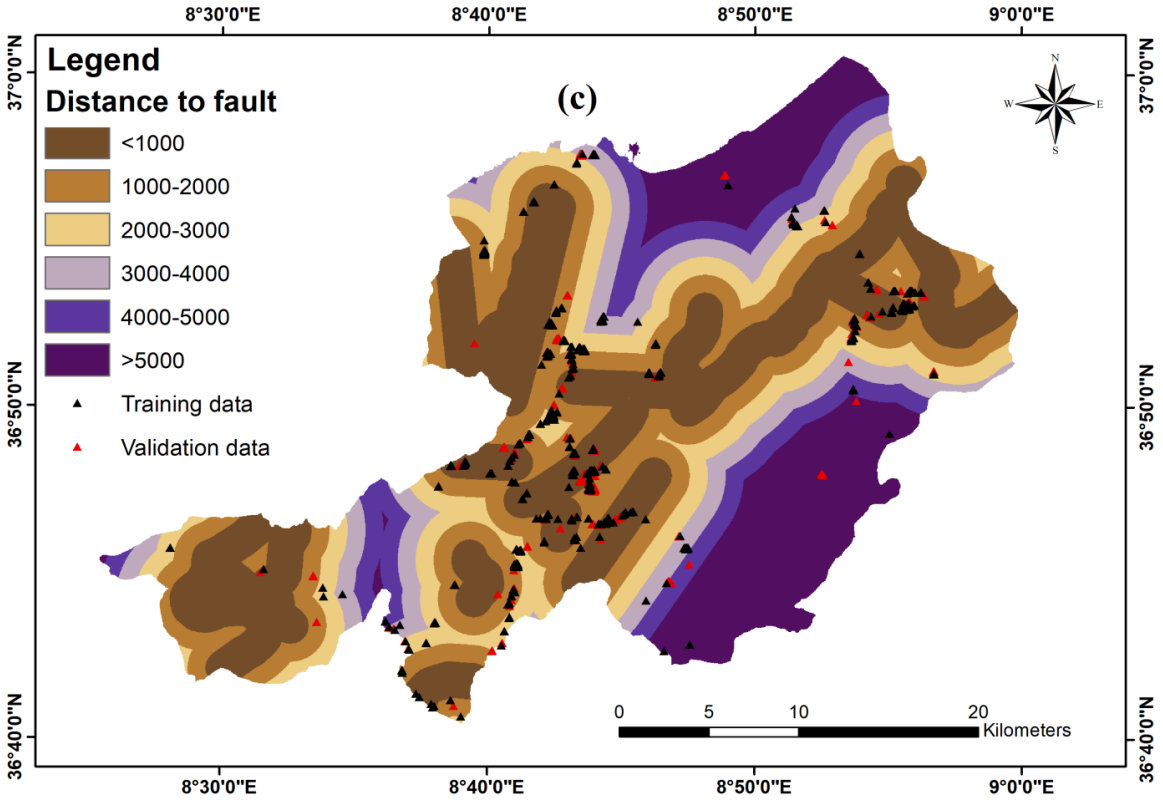

Figure 2c: Landslide conditioning factors – distance to fault

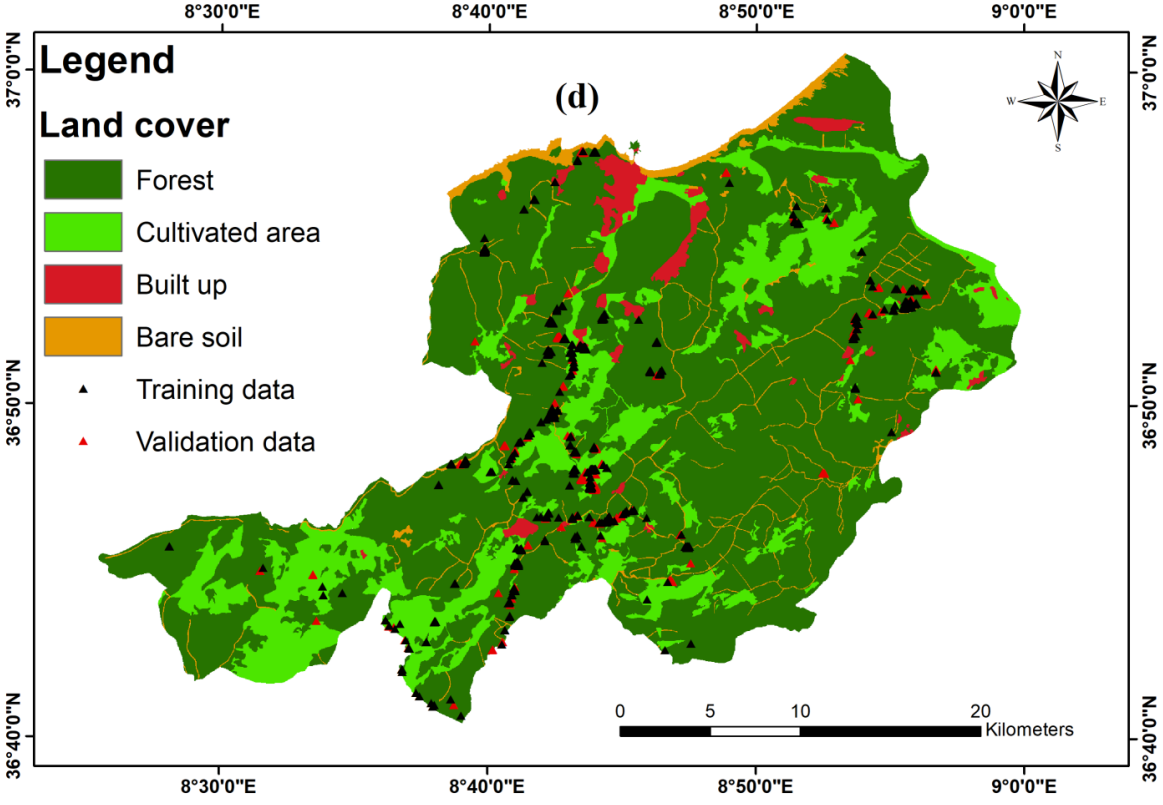

Figure 2d: Landslide conditioning factors – land cover/use

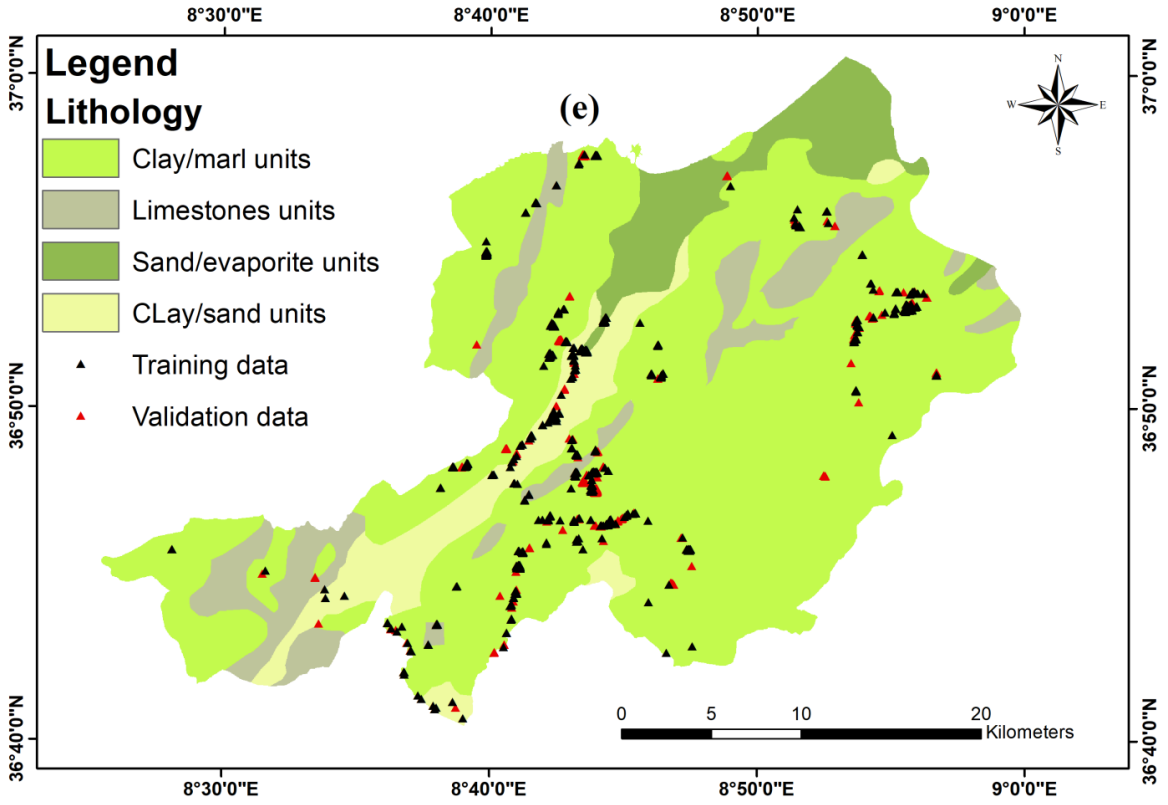

Figure 2e: Landslide conditioning factors – lithology

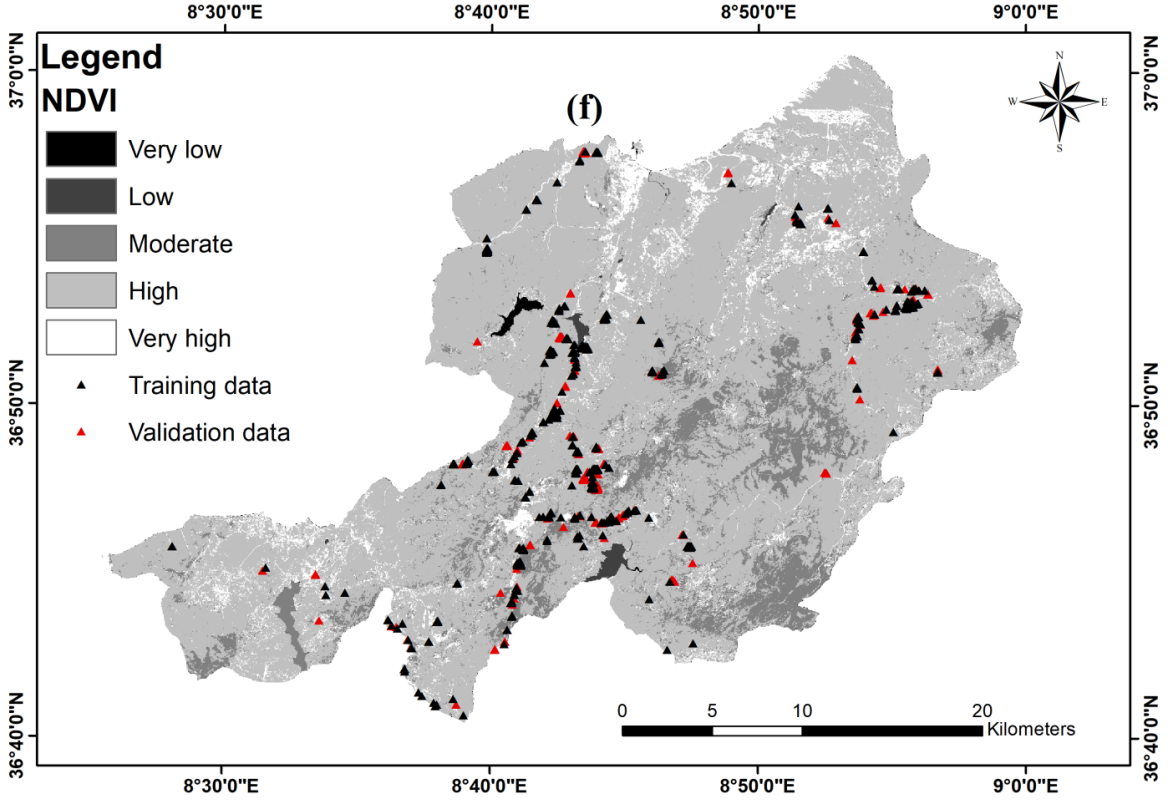

Figure 2f: Landslide conditioning factors – NDVI

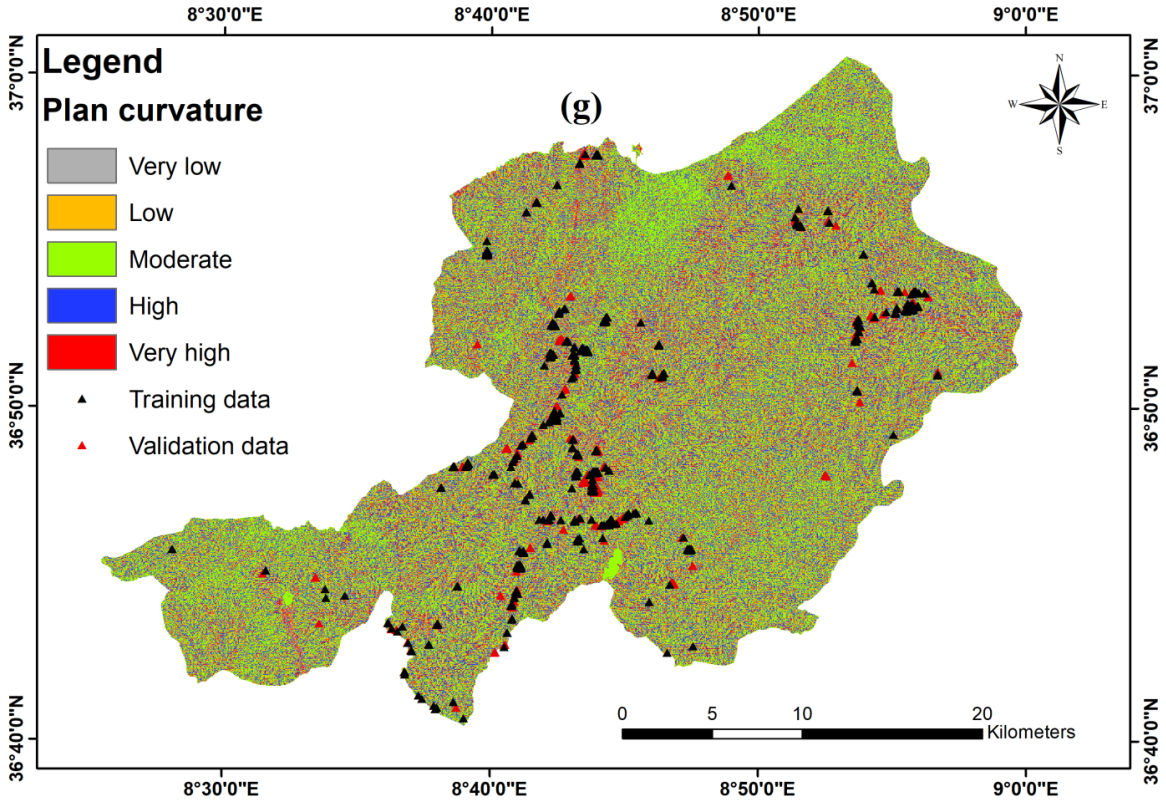

Figure 2g: Landslide conditioning factors – plan curvature

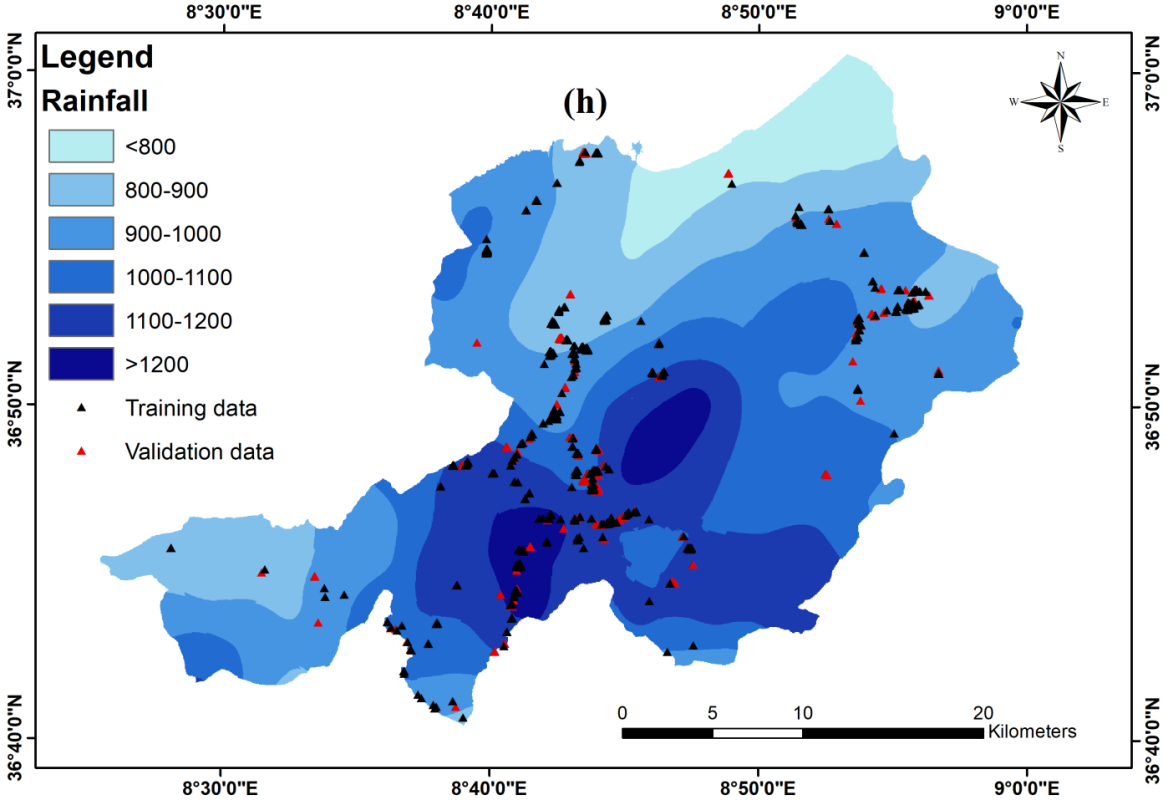

Figure 2h: Landslide conditioning factors – rainfall

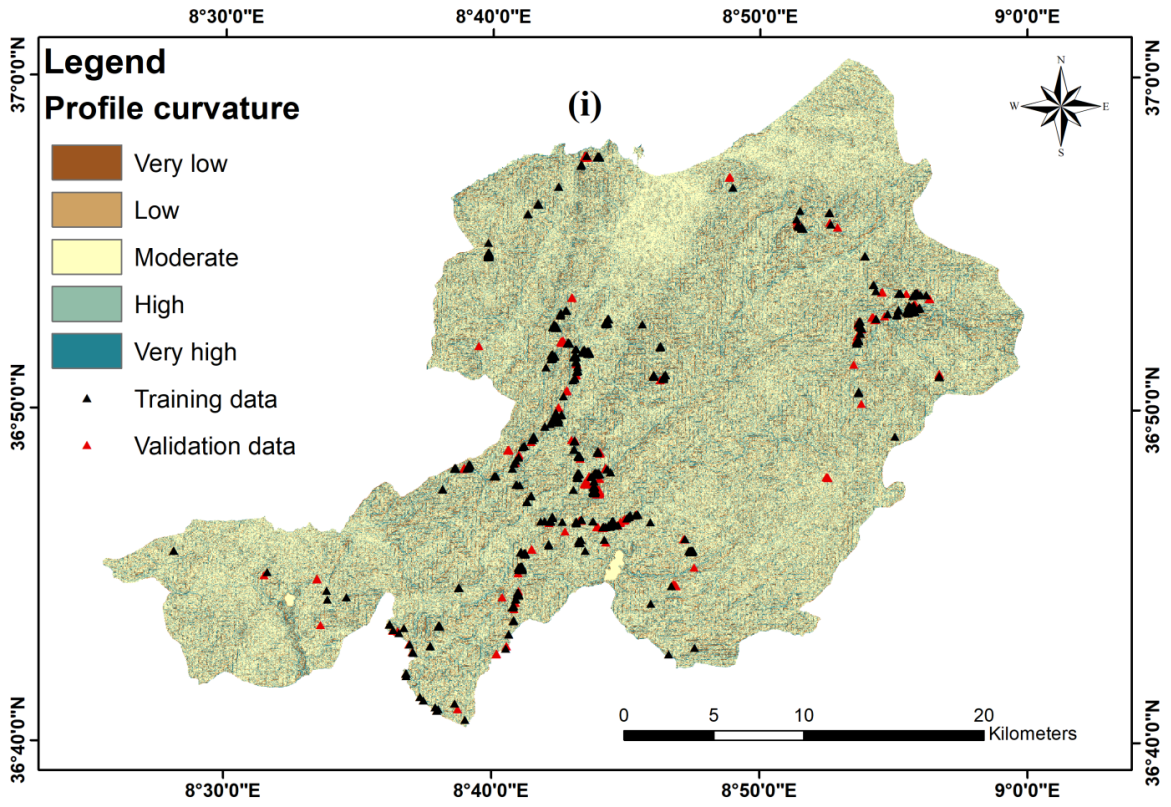

Figure 2i: Landslide conditioning factors – profile curvature

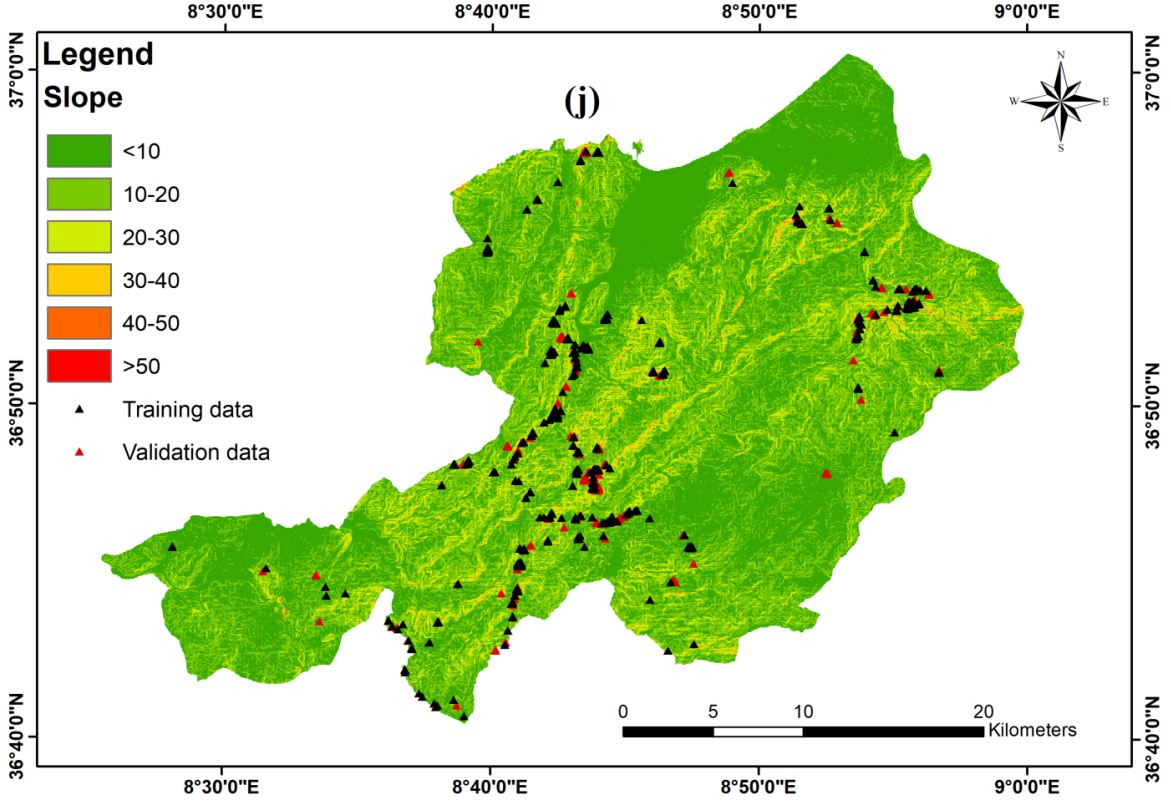

Figure 2j: Landslide conditioning factors – slope

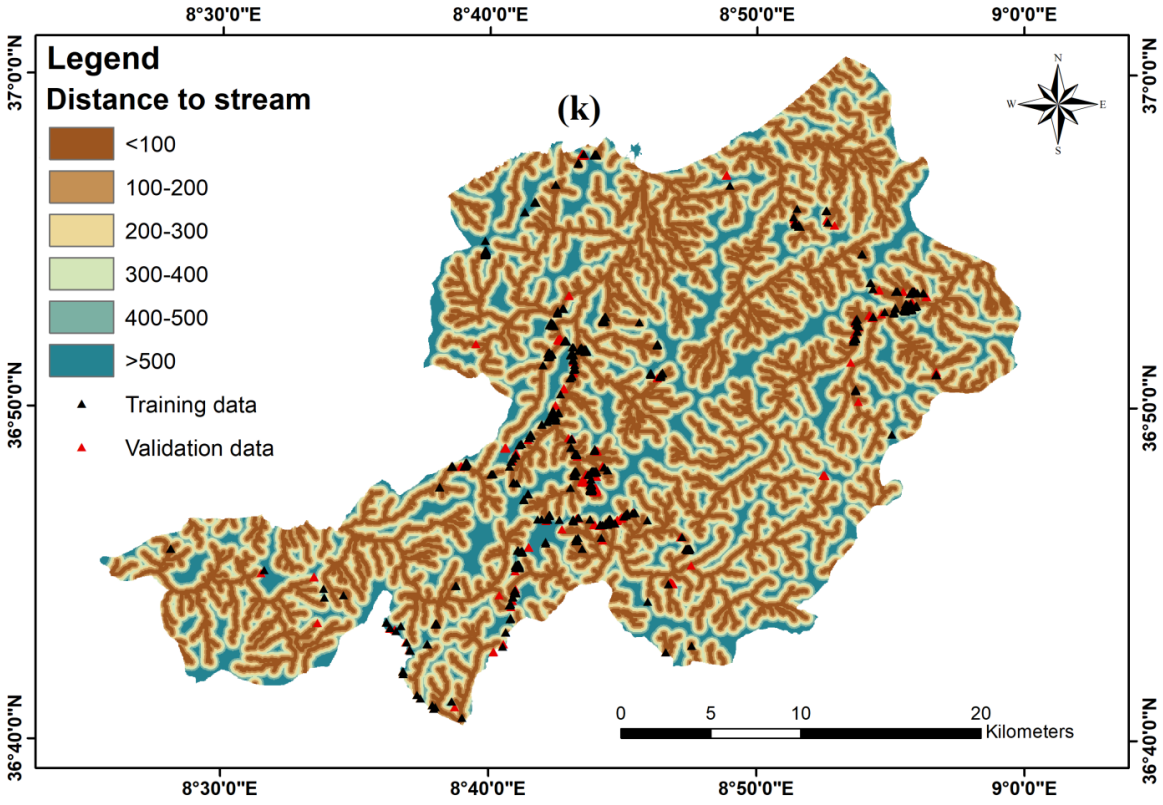

Figure 2k: Landslide conditioning factors – distance to drainage network

247.5°), west (247.5°-292.5°) and northwest (292.5°-337.5°) (Figure 2a).

3.6 Plan curvature

Plan curvature is a geometrical parameter of the earth surface; it describes the slope change in inclination or aspect [58]. Plan curvature was also derived from DEM (30x30) and reclassified into five classes (natural break from Jenks) : <-0.74 (very low), from -0.74 to-0.23 (low), from −0.23 to 0.16 (moderate), from 0.16 to 0.67 (high), >0.67 (very high) (Figure 2g).

3.7 Profile curvature

The curvature in the vertical plane parallel to the slope direction is considered as the profile curvature and it was usually used in susceptibility mapping [59]. Profile curvature was also derived from DEM and reclassified into five classes (natural break) :<−0.99 (very low), from −0.99 to −0.34 (low), from −0.34 to 0.16 (moderate), from 0.16 to 0.81 (high) and >0.81 (very high) (Figure 2i).

3.8 Distance to drainage network

Rivers and drainage networks play an important role in landslide occurrence since they accumulate waters and saturate the surrounded surface and subsurface area [39, 60, 61]. In this study, a drainage network was derived from DEM, and then the distance to drainage was generated by Euclidean distance in ARCGIS 10.4 software. Finally, the distance to drainage was reclassified into six classes with a 100m interval: <100m, 100m-200m, 200m-300m, 300m-400m, 400m-500m, >500m (Figure 2k).

3.9 NDVI

The normalized difference vegetation index (NDVI) was extracted from Sentinel 2A satellite image [28] and calculated by the following equation:

$$NDVI = \frac{IR - R}{IR + R} \quad (1)$$

Where, IR is the infrared and R is the red bands of the electromagnetic spectrum. In this study, NDVI varies from −0.11 to 0.48 and it was reclassified into five classes (natural breaks from Jenks) : <0 (very low), 0-0.32 (low), 0.32-

0.48 (moderate), 0.48-0.61 (high) and >0.61 (very high) (Figure 2f).

3.10 Land use/cover

The land use/cover map of the study area was derived from the interpretation of Sentinel 2A satellite image using the semi automatic classification plugin in Qgis [62] and also based on Regional Commissariat for Agricultural Development of Jendouba [63] maps and data. The land use/cover map was reclassified into four classes: forest, cultivated area, bare soil and built up (Figure 2d).

3.11 Distance to fault

The strength of rocks decreases with the amount of joints, which increase with the distance to faults. Thus, the distance to fault was considered as landslide susceptibility mapping factor [48, 64].

Fault map was derived from geological map of the National Office of Mines [65], the Euclidean distance was applied to generate the distance to fault map, then reclassified into six classes with 1000m of interval: <1000m, 1000m-2000m, 2000m-3000m, 3000m-4000m, 4000m-5000m, >5000m (Figure 2c).

3.12 Lithology

The lithology has an important impact on slope stability, the different lithological units have different susceptibility degree [66–68]; for example, clay unit is more prone to fail than calcareous unit. With this logic in mind, the lithological map was derived from the geological map and was reclassified into four classes: clay and marl units, clay and sand units, sand and evaporates units and limestone and calcareous units from the most to the least susceptible, respectively (Figure 2e).

3.13 Rainfall

Rainfall is considered as the landslide triggering factor. It plays an important role in shear strength decrease by increasing pore pressure [69]. Thus, rainfall is usually used in susceptibility analysis [28, 70, 71]. The annual average precipitation map was produced by kriging data of meteorological stations available in Tabarka and Ain-Drahim delegations Then, reclassified into six classes with 100mm/year interval: <800, 800-900, 900-1000, 1000-1100, 1100-1200, >1200 mm/year (Figure 2h).

4 Methodology

In this study two statistical bivariate models: evidential belief function (EBF) and weight of evidence (WoE) were used to produce landslide susceptibility maps using ARCGIS 10.4 as GIS software.

4.1 Evidential belief function (EBF)

The theory of belief functions is a statistical bivariate model known as Dempster-Shafer theory [72, 73]. The evidential belief function has been used in landslide susceptibility mapping by many researchers [6, 30, 32]. The EBF model is defined by four statistical functions: Bel (degree of belief) which means the lower degree of belief for each factor, Dis (degree of disbelief) which means the degree of disbelief for each factor, Unc (degree of uncertainty) which means the degree of uncertainty for each factor and Pls (degree of plausibility) which means the upper limits of the probability. The data driven estimation of the evidential belief functions can be calculated by many equations; in this study, the equations used by researchers which include [31, 74] were applied.

4.2 Weight of evidence (WoE)

The weight of evidence method was used for the first time in 1988 for mineral exploration [75] and in 2003 for landslide susceptibility mapping [76]. Then, the WoE method was widely used by researchers [6, 77–80]. The WoE method is a probabilistic method based on the following Bayes' rule equations:

$$P(AB) = P(BA) \times \frac{P(A)}{P(B)} \tag{2}$$

4.3 Validation of landslide susceptibility models

After elaborating the landslide susceptibility map using different models, their validation is necessary in order to check their reliability, to compare the results of these models and to choose the best one. There are many method of model validation such as: success/ prediction rate curve,

landslide density or frequency, Chi squared, etc. The success/prediction rate curve is the most common method followed by landslide density or frequency [81]. In this study, both success and predictive rate curves using the area under the receiver operating characteristic curve (AUROC) were applied.

The success rate curve allow to check how well the resultant map has classified the areas of existing landslides [82]. The success rate curve was obtained by comparing the training dataset with the landslide susceptibility map.

The prediction rate curve indicates the model efficiency to predict future landslide [17, 83]. The comparison of the validation dataset with the landslide susceptibility map provides the prediction rate curve.

5 Results

5.1 Conditioning factors

The weights of all classes of all conditioning factors calculated with the EBF and WoE models are presented in the first table (Table 1). Results show a good correlation between the weights of each class for the two models. This indicates that the susceptibility of each class is similar for all methods.

The highest susceptible classes of the aspect is SW followed by E. Also the S and SE classes have an effect on landslide triggering but less than SW and E classes.

For the elevation factor, the highest weight values are for the 600-800 m asl class followed by the <200 m asl class for the EBF model. But, for the WoE model it is the reverse, the highest weight is for the <200 m asl class followed by the 600-800 m asl class.

The most susceptible classes of the distance to fault factor is the 1000-2000m class followed by the <1000m class and the 2000-3000m class.

The clay/sand lithological units are the most susceptible class followed by the clay/marl units for all the two models.

The land cover/use factor shows that the built up is the most susceptible classes followed by the cultivated area and the bare soil classes.

Concerning the NDVI factor, the most susceptible class is the low class followed by the very low class. The NDVI low class have the highest value of all classes of all factors.

For the plan curvature and the profile curvature factors the highest values are for the very low and the very high classes.

Regarding the rainfall factor, as expected, the most susceptible class is the>1200 mm/year class followed by the 1100-1200 mm/year class, the landslide density increase as the rainfall increase.

With regard to the slope factor, the highest weights are for the 40-50° and >50° classes (they have similar weights) followed by the 30-40° class for the EBF model. For the WoE model the highest weight is for the 40-50° class followed by 30-40° and >50° classes, respectively.

Finally, the most susceptible class for the distance to drainage factor is the <100m class and the weights of classes decrease by moving away from the drainage network

5.2 Application of statistical models

The LSI values range between 1.03 and 3.6 for EBF model, and between −54.72 and 90.56 for the WoE model. The lower the LSI pixel value the less the pixel is susceptible to landslide. The output landslide susceptibility map (LSM) was produced and classified into five classes using the natural breaks (Jenks) method: very low, low, moderate, high and very high for the two models (Figure 3).

In the current study, the area percentage of each class is shown in (Table 2). In the case of the EBF model, the distribution of class area was as following: 15.77% for the very low class, 33.25% for the low class, 32.4% for the moderate class, 13.96% for the high class and 4.62% for the very high class. As regards to the WoE model, the very low, low, moderate, high and very high classes has 18.96%, 33.82%, 28.83%, 12.83% and 5.56% of the entire study area, respectively. Result shows that the spatial distribution of the susceptibility is very similar.

5.3 Validation of models

The validation and the check of the capabilities of the LSM produced by the two models were carried out with both success and prediction rate curves. ROC curves were plotted by comparing the LSM with the training and the validating data set of the inventory map and the area under the ROC curves was calculated. Result shows that the AUC of the success rate curves were 0.879 for the EBF model and 0.895 for the WoE model (Figure 4a). The AUC of the prediction rate curves were 0.848 for the EBF model and 0.865 for the WoE model (Figure 4b). The AUC of the success rate and predictive rate curves range between 0.8-0.9 indicating a good performance of the two models [84].

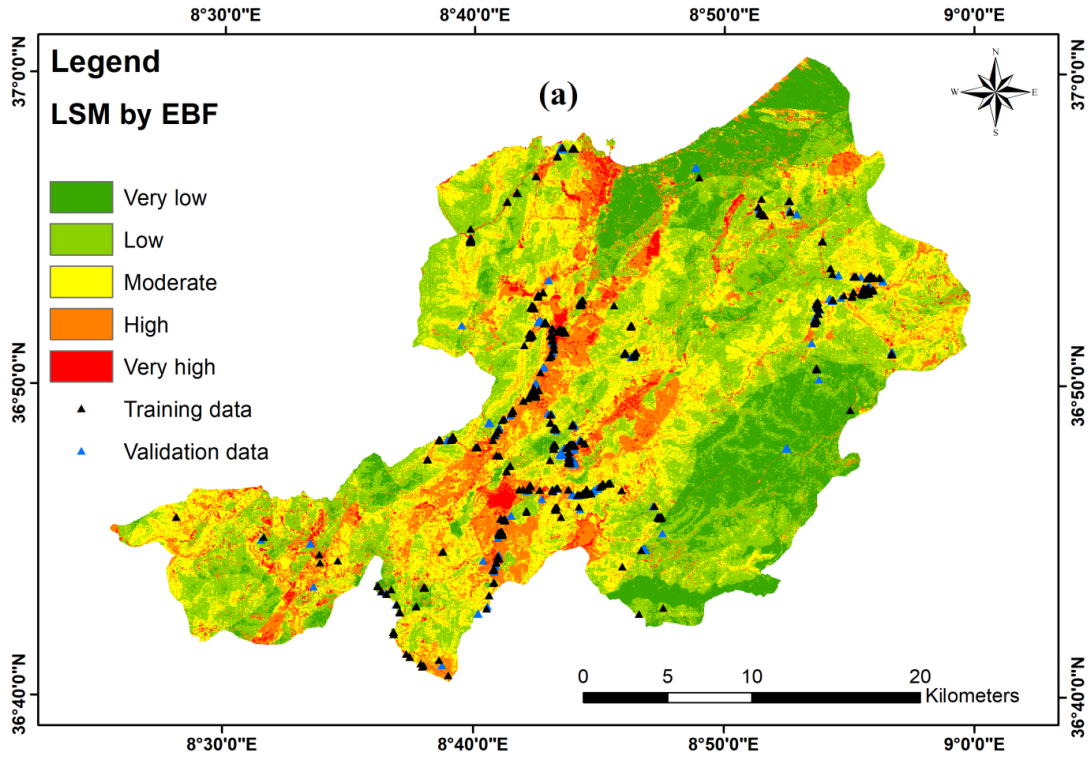

(a)

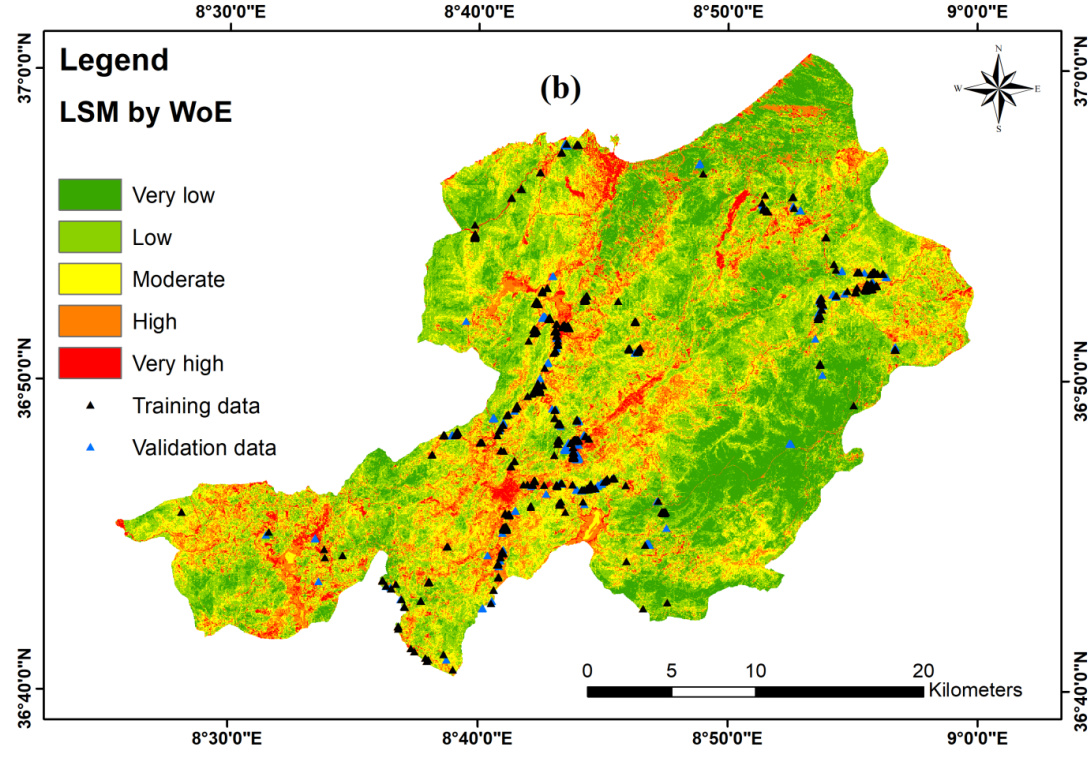

(b)

Figure 3: LSMs of the EBF (a) and WoE (b) models.

Table 1: Spatial relationship between each landslide conditioning factor and landslide by EBF and WoE models.

Factor	Class	N. of class pixels	N. of landslide pixels	Percentage of class	Percentage of landslide	Bel	Dis	Unc	Pls	C	S(C)	C/ S(C)
Aspect	Flat	2177	1	0.19	0.13	0.071	0.111	0.818	0.889	−0.442	1.001	−0.441
	N	172221	75	15.39	9.39	0.067	0.119	0.814	0.881	−0.563	0.121	−4.638
	NE	124452	47	11.12	5.88	0.058	0.118	0.824	0.882	−0.694	0.150	−4.615
	E	132827	124	11.87	15.52	0.144	0.106	0.750	0.894	0.311	0.098	3.177
	SE	134463	120	12.01	15.02	0.138	0.107	0.755	0.893	0.258	0.099	2.604
	S	122931	106	10.98	13.27	0.133	0.108	0.759	0.892	0.215	0.104	2.059
	SW	103423	140	9.24	17.52	0.209	0.101	0.690	0.899	0.736	0.093	7.899
	W	144238	101	12.89	12.64	0.108	0.111	0.781	0.889	−0.022	0.106	−0.208
	NW	182477	85	16.30	10.64	0.072	0.119	0.810	0.881	−0.492	0.115	−4.291
DEM	<200	310162	277	27.71	34.67	0.287	0.181	0.533	0.819	0.325	0.074	4.372
	200_400	280221	174	25.04	21.78	0.199	0.209	0.592	0.791	−0.182	0.086	−2.124
	400_600	352146	206	31.46	25.78	0.188	0.216	0.596	0.784	−0.279	0.081	−3.446
	600_800	147623	140	13.19	17.52	0.304	0.190	0.506	0.810	0.335	0.093	3.600
	>800	29057	2	2.60	0.25	0.022	0.205	0.773	0.795	−2.363	0.708	−3.337
Fault	>5000	193650	4	17.30	0.50	0.005	0.201	0.793	0.799	−3.728	0.501	−7.437
	4000_5000	88507	8	7.91	1.00	0.024	0.180	0.796	0.820	−2.139	0.355	−6.019
	3000_4000	109585	85	9.79	10.64	0.206	0.166	0.629	0.834	0.092	0.115	0.805
	2000_3000	156175	134	13.95	16.77	0.227	0.162	0.611	0.838	0.217	0.095	2.292
	1000_2000	247963	289	22.16	36.17	0.309	0.137	0.554	0.863	0.689	0.074	9.349
	<1000	323319	279	28.89	34.92	0.229	0.153	0.618	0.847	0.278	0.074	3.747
Geology	Limestones	122056	33	10.91	4.13	0.097	0.273	0.629	0.727	−1.044	0.178	−5.873
	Sand/Evaporite	89705	46	8.02	5.76	0.184	0.260	0.555	0.740	−0.355	0.152	−2.338
	Clay/ Sand	94411	119	8.44	14.89	0.453	0.236	0.311	0.764	0.642	0.099	6.453
	Clay/ Marl	813001	601	72.64	75.22	0.266	0.230	0.504	0.770	0.134	0.082	1.632
Land Cover	Forest	824871	525	73.71	65.71	0.147	0.309	0.543	0.691	−0.381	0.075	−5.108
	Bare soils	40397	32	3.61	4.01	0.183	0.236	0.581	0.764	0.108	0.180	0.598
	Cultivated	225037	182	20.11	22.78	0.187	0.229	0.584	0.771	0.159	0.084	1.879
	Built up	28714	60	2.57	7.51	0.483	0.225	0.292	0.775	1.126	0.134	8.379
NDVI	Very low	11246	24	1.00	3.00	0.221	0.184	0.595	0.816	1.115	0.207	5.376
	Low	70754	442	6.32	55.32	0.646	0.090	0.265	0.910	2.909	0.071	40.825
	Moderate	216910	203	19.38	25.41	0.097	0.174	0.729	0.826	0.348	0.081	4.285
	High	340479	101	30.42	12.64	0.031	0.236	0.734	0.764	−1.106	0.106	−10.386
	Very high	479772	29	42.87	3.63	0.006	0.317	0.677	0.683	−2.992	0.189	−15.816
Plan curvature	Very low	70102	77	6.26	9.64	0.273	0.192	0.535	0.808	0.468	0.120	3.898
	Low	263475	196	23.54	24.53	0.185	0.196	0.619	0.804	0.054	0.082	0.659
	Moderate	395776	236	35.36	29.54	0.148	0.217	0.635	0.783	−0.266	0.078	−3.433
	High	296301	207	26.47	25.91	0.174	0.200	0.626	0.800	−0.029	0.081	−0.363
	Very high	93555	83	8.36	10.39	0.220	0.195	0.585	0.805	0.240	0.116	2.066
Rainfall	<800	78940	1	7.05	0.13	0.003	0.179	0.818	0.821	−4.104	1.001	−4.101

Table 1: ...continued

Factor	Class	N. of class pixels	N. of landslide pixels	Percentage of class	Percentage of landslide	Bel	Dis	Unc	Pls	C	S(C)	C/ S(C)
	800_900	206417	167	18.44	20.90	0.179	0.162	0.659	0.838	0.156	0.087	1.789
	900_1000	333245	237	29.78	29.66	0.158	0.167	0.675	0.833	−0.005	0.077	−0.070
	1000_1100	246279	134	22.00	16.77	0.121	0.178	0.702	0.822	−0.337	0.095	−3.553
	1100_1200	207694	189	18.56	23.65	0.202	0.156	0.642	0.844	0.307	0.083	3.690
	>1200	46634	71	4.17	8.89	0.338	0.158	0.504	0.842	0.808	0.124	6.493
Profile curvature	Very low	56284	42	5.03	5.26	0.189	0.199	0.612	0.801	0.047	0.159	0.294
	Low	221189	157	19.76	19.65	0.180	0.199	0.621	0.801	−0.007	0.089	−0.080
	Moderate	426456	272	38.10	34.04	0.162	0.212	0.626	0.788	−0.176	0.075	−2.360
	High	328260	227	29.33	28.41	0.175	0.202	0.623	0.798	−0.045	0.078	−0.570
	Very high	87020	101	7.78	12.64	0.294	0.189	0.517	0.811	0.540	0.107	5.071
Slope	<10	519673	291	46.43	36.42	0.014	0.194	0.792	0.806	−0.414	0.074	−5.632
	10_20	470256	305	42.02	38.17	0.016	0.175	0.809	0.825	−0.160	0.073	−2.198
	20_30	112814	137	10.08	17.15	0.030	0.151	0.819	0.849	0.613	0.094	6.528
	30_40	15083	39	1.35	4.88	0.064	0.158	0.778	0.842	1.323	0.164	8.051
	40_50	1320	26	0.12	3.25	0.485	0.159	0.356	0.841	3.349	0.201	16.640
	>50	63	1	0.01	0.13	0.391	0.164	0.445	0.836	3.103	1.009	3.077
Drainage	>500	103202	32	9.22	4.01	0.081	0.177	0.742	0.823	−0.890	0.180	−4.931
	400_500	105408	65	9.42	8.14	0.161	0.170	0.669	0.830	−0.160	0.129	−1.240
	300_400	153319	80	13.70	10.01	0.136	0.175	0.689	0.825	−0.355	0.118	−3.014
	200_300	193542	108	17.29	13.52	0.146	0.175	0.679	0.825	−0.291	0.104	−2.811
	100_200	246063	222	21.99	27.78	0.236	0.155	0.609	0.845	0.311	0.079	3.941
	<100	317675	292	28.38	36.55	0.240	0.148	0.612	0.852	0.374	0.073	5.085

N: number, Bel : belief function, Dis : disbelief function, Pls: Plausibility, C: contrast and S(C): variance of contrast.

Table 2: Distribution of class area and landslide using natural breaks method

Susceptibility	EBF		WoE	
	Area (%)	Landslide (%)	Area (%)	Landslide (%)
very low	15.77	1.00	18.96	0.73
low	33.25	5.18	33.82	4.55
moderate	32.40	18.45	28.83	14.27
high	13.96	22.00	12.83	25.09
very high	4.62	53.36	5.56	55.36

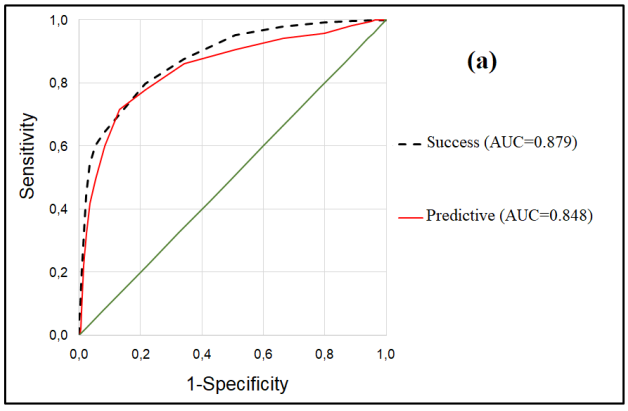

(a)

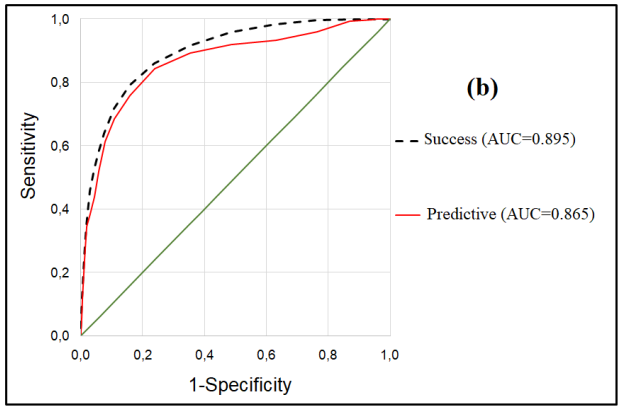

(b)

Figure 4: Success and predictive ROC curves (a) EBF and (b) WoE

6 Discussion

In landslide susceptibility bivariate statistics-based method, the preparation of data is very important. Especially, landslide inventory map since all statistics are based on quantities and landslide distribution in the study area. The relationship between conditioning factors and landslide releases is also very important. Based on EBF and WoE as two bivariate statistics method, the weights of all classes of all conditioning factors maps were calculated to reveal the relationship between landslide and every conditioning factor for the present study area. Results show that the susceptibility of each class is similar by the two models indicating that if a factor class is susceptible for landslide, it must have a high weight for any statistical method [28].

In the present study, results show that the most susceptible class of the aspect factor was the SW followed by the E, S and SE classes. This may be due to the dry and warm summer wind coming from the S and/or the SE Tunisian prevailing wind. In summers, these slopes are exposed to warm wind, therefore clay lithological units shrink and drying slots appear which facilitates the wind and rainfall infiltration. This process leads to a deep and quick alteration of clay units which become more prone to landslide.

For the elevation there was no specific correlation between the altitude and landslide. The most susceptible class was 600-800m asl which has a medium elevation in the study area. Many researchers reveal that susceptibility is low for higher elevation due to the presence of bedrocks resistant to weathering processes [19, 55]. The high weight of the <200m asl class is due to the fact that low elevation accumulate loosely consolidated components of erosion scraps and screeds [85].

Concerning the linear distance to fault factor there is no clear relationship with landslide, this may be due to the infrequent tectonic activity in the study area.

With regards to the relationship between landslide and lithological units, the most susceptible class was the clay/sand units followed by the clay/marl units which indicate the effect of clay on landslide triggering. The alternation of sand with clay beds may increase the susceptibility to landslide by accumulating the rainfalls water for long times which decrease the shear strength of clay beds. Also, the presence of sand as loose material in slopes can come in as a sliding surface during rainfall.

Regarding the plan curvature and profile curvature factors, the susceptible classes were the extreme classes (concave and convex), which is logical because the increase of slope convexity increase the landslide susceptibility; also concavity and convexity are two mutual parameters.

Classes with high precipitation of rainfall factor were more susceptible. Indeed, rainfall increase the water content of clay formation which increase the pore pressure and decrease the shear strength of clay units [69]. Also water play as lubricant of clay minerals which facilitates their sliding [86].

As expected the high slope angle classes were more susceptible, the 40°-50° class was the most susceptible fol-

lowed by the >50° class due to the small area of the >50° class (0.01% of the study area). For the WoE model, the 30°-40° class was more susceptible than the >50° class owing to the high variance of this class (one landslide pixel). Generally, landslide susceptibility increase as the slope angle increase on account of the increasing of shear stress of soil.

Concerning the linear distance to drainage network, the landslide susceptibility increases inversely proportional to the distance. Drainage networks accumulate the erosion remains which are loose material. Also, the drainage networks increase the water content of adjacent soils by accumulating rainfalls water.

For the land cover/use, the most susceptible class was the built up class followed by the cultivated area and bare soil classes. The forest class is the least susceptible class by dint of tree roots which fixes the soil, this is why bare soils were more susceptible than forest. The susceptibility of the cultivated area class can be attributed to the irrigation and the very loose soil in slope. The very high susceptibility of the built up class is due to the disruption of natural slope by the house building and especially the road construction in slope area without strong geotechnical studies. This was in line with the NDVI classes weights. In fact, the low class of NDVI factor was the most susceptible which can be attributed to the buildings (constructions and roads) because the very low class may attributed to water accumulation in rivers.

In this study, two LSMs were established using EBF and WoE as bivariate statistical models. Results show a very good accuracy of the EBF and WoE models. The WoE success rate and predictive rate are more than the EBF model indicating that the WoE model can be more efficient than the EBF model for the current study.

7 Conclusion

The Tabarka/ Ain-Drahim region in the North western area of Tunisia present several landslides every year which cause damages to infrastructures and properties. In this study, 11 conditioning factors were prepared: aspect, elevation, rainfall, lithology, slope, distance to drainage network, distance to fault, plan curvature, profile curvature, NDVI and land cover/use. Using aerial photo and extent field investigation, an inventory map of landslides, that have occurred since 2004, was produced and 451 landslides have been located. A randomly selection of 316 landslides, which represent 70% of all landslides, were used to produce landslide susceptibility models and 135 landslides (30%) were used to validate models.

The statistical relationship between conditioning factors and landslides was studied using the inventory map. The low NDVI class (judged as buildings) and the built up land cover/use class had the highest weights. The anthropogenic factor by the disturbance of natural slope is the main cause of landslides in the study area.

A GIS-based EBF and WoE bivariate statistical models were applied. In order to check and validate the capabilities of models both success and predictive rates using AUROC curve were calculated. The success rates and predictive rates of the two models were about 90% showing a good performance of models and good capabilities in predicting future landslides for the current study area.

The landslide susceptibility map of the WoE model was deemed to be the best map and it may be useful in the future especially in geotechnical planning to help avoiding the existing mistakes.

References

[1] Del Ventisette C, Garfagnoli F, Ciampalini A, et al. Catastrophic debris-flows: geological hazard and human influence. EGU General Assembly Conference Abstracts; 2013.
[2] Aleotti P, Chowdhury R. Landslide hazard assessment: summary review and new perspectives. Bulletin of Engineering Geology and the environment 1999;58:21-44.
[3] NDDL. https://unictunis.org.tn/category/catastrophes-naturelles/. 2012.
[4] Ayalew L, Yamagishi H. The application of GIS-based logistic regression for landslide susceptibility mapping in the Kakuda-Yahiko Mountains, Central Japan. Geomorphology 2005;65:15-31.
[5] Constantin M, Bednarik M, Jurchescu MC, Vlaicu M. Landslide susceptibility assessment using the bivariate statistical analysis and the index of entropy in the Sibiciu Basin (Romania). Environmental earth sciences 2011;63:397-406.
[6] Cui K, Lu D, Li W. Comparison of landslide susceptibility mapping based on statistical index, certainty factors, weights of evidence and evidential belief function models. Geocarto International 2017;32:935-55.
[7] Guzzetti F, Reichenbach P, Cardinali M, Galli M, Ardizzone F. Probabilistic landslide hazard assessment at the basin scale. Geomorphology 2005;72:272-99.
[8] Pradhan B. Landslide susceptibility mapping of a catchment area using frequency ratio, fuzzy logic and multivariate logistic regression approaches. Journal of the Indian Society of Remote Sensing 2010;38:301-20.
[9] Guzzetti F, Carrara A, Cardinali M, Reichenbach P. Landslide hazard evaluation: a review of current techniques and their application in a multi-scale study, Central Italy. Geomorphology 1999;31:181-216.
[10] Soeters R, Van Westen CJ. Landslides: Investigation and mitigation. Chapter 8-Slope instability recognition, analysis, and zonation. Transportation research board special report 1996.

[11] Thiery Y, Malet J-P, Sterlacchini S, Puissant A, Maquaire O. Analyse spatiale de la susceptibilité des versants aux glissements de terrain. Revue Internationale de Géomatique 2005;15:227-45.
[12] Van Westen CJ. The modelling of landslide hazards using GIS. Surveys in Geophysics 2000;21:241-55.
[13] Bourenane H, Bouhadad Y, Guettouche MS, Braham M. GIS-based landslide susceptibility zonation using bivariate statistical and expert approaches in the city of Constantine (Northeast Algeria). Bulletin of Engineering Geology and the Environment 2015;74:337-55.
[14] Chen W, Li W, Chai H, Hou E, Li X, Ding X. GIS-based landslide susceptibility mapping using analytical hierarchy process (AHP) and certainty factor (CF) models for the Baozhong region of Baoji City, China. Environmental Earth Sciences 2016;75:63.
[15] Hadji R, Achour Y, Hamed Y. Using GIS and RS for Slope Movement Susceptibility Mapping: Comparing AHP, LI and LR Methods for the Oued Mellah Basin, NE Algeria. Euro-Mediterranean Conference for Environmental Integration; 2017: Springer. p. 1853-6.
[16] Achour Y, Boumezbeur A, Hadji R, Chouabbi A, Cavaleiro V, Bendaoud EA. Landslide susceptibility mapping using analytic hierarchy process and information value methods along a highway road section in Constantine, Algeria. Arabian Journal of Geosciences 2017;10:194.
[17] Pradhan B, Lee S. Delineation of landslide hazard areas on Penang Island, Malaysia, by using frequency ratio, logistic regression, and artificial neural network models. Environmental Earth Sciences 2010;60:1037-54.
[18] Nourani V, Pradhan B, Ghaffari H, Sharifi SS. Landslide susceptibility mapping at Zonouz Plain, Iran using genetic programming and comparison with frequency ratio, logistic regression, and artificial neural network models. Natural hazards 2014;71:523-47.
[19] Zare M, Pourghasemi HR, Vafakhah M, Pradhan B. Landslide susceptibility mapping at Vaz Watershed (Iran) using an artificial neural network model: a comparison between multilayer perceptron (MLP) and radial basic function (RBF) algorithms. Arabian Journal of Geosciences 2013;6:2873-88.
[20] Peng L, Niu R, Huang B, Wu X, Zhao Y, Ye R. Landslide susceptibility mapping based on rough set theory and support vector machines: A case of the Three Gorges area, China. Geomorphology 2014;204:287-301.
[21] Kalantar B, Pradhan B, Naghibi SA, Motevalli A, Mansor S. Assessment of the effects of training data selection on the landslide susceptibility mapping: a comparison between support vector machine (SVM), logistic regression (LR) and artificial neural networks (ANN). Geomatics, Natural Hazards and Risk 2018;9:49-69.
[22] Bui DT, Pradhan B, Lofman O, Revhaug I, Dick OB. Landslide susceptibility mapping at Hoa Binh province (Vietnam) using an adaptive neuro-fuzzy inference system and GIS. Computers & Geosciences 2012;45:199-211.
[23] Sdao F, Lioi D, Pascale S, Caniani D, Mancini I. Landslide susceptibility assessment by using a neuro-fuzzy model: a case study in the Rupestrian heritage rich area of Matera. Natural hazards and earth system sciences 2013;13:395.
[24] Liu M, Chen X, Yang S. Collapse landslide and mudslides hazard zonation. Landslide science for a safer geoenvironment: Springer; 2014:457-62.
[25] Ilia I, Koumantakis I, Rozos D, Koukis G, Tsangaratos P. A geographical information system (GIS) based probabilistic certainty factor approach in assessing landslide susceptibility: the case study of Kimi, Euboea, Greece. Engineering Geology for Society and Territory-Volume 2: Springer; 2015:1199-204.
[26] Regmi AD, Devkota KC, Yoshida K, et al. Application of frequency ratio, statistical index, and weights-of-evidence models and their comparison in landslide susceptibility mapping in Central Nepal Himalaya. Arabian Journal of Geosciences 2014;7:725-42.
[27] Kavzoglu T, Sahin EK, Colkesen I. An assessment of multivariate and bivariate approaches in landslide susceptibility mapping: a case study of Duzkoy district. Natural Hazards 2015;76:471-96.
[28] Vakhshoori V, Zare M. Landslide susceptibility mapping by comparing weight of evidence, fuzzy logic, and frequency ratio methods. Geomatics, Natural Hazards and Risk 2016;7:1731-52.
[29] Youssef AM, Al-Kathery M, Pradhan B. Landslide susceptibility mapping at Al-Hasher area, Jizan (Saudi Arabia) using GIS-based frequency ratio and index of entropy models. Geosciences Journal 2015;19:113-34.
[30] Pradhan B, Abokharima MH, Jebur MN, Tehrany MS. Land subsidence susceptibility mapping at Kinta Valley (Malaysia) using the evidential belief function model in GIS. Natural hazards 2014;73:1019-42.
[31] Bui DT, Pradhan B, Lofman O, Revhaug I, Dick OB. Spatial prediction of landslide hazards in Hoa Binh province (Vietnam): a comparative assessment of the efficacy of evidential belief functions and fuzzy logic models. Catena 2012;96:28-40.
[32] Zhang Z, Yang F, Chen H, et al. GIS-based landslide susceptibility analysis using frequency ratio and evidential belief function models. Environmental Earth Sciences 2016;75:948.
[33] Xu C, Xu X, Dai F, Xiao J, Tan X, Yuan R. Landslide hazard mapping using GIS and weight of evidence model in Qingshui river watershed of 2008 Wenchuan earthquake struck region. Journal of Earth Science 2012;23:97-120.
[34] Lepore C, Kamal SA, Shanahan P, Bras RL. Rainfall-induced landslide susceptibility zonation of Puerto Rico. Environmental Earth Sciences 2012;66:1667-81.
[35] Felicísimo ÁM, Cuartero A, Remondo J, Quirós E. Mapping landslide susceptibility with logistic regression, multiple adaptive regression splines, classification and regression trees, and maximum entropy methods: a comparative study. Landslides 2013;10:175-89.
[36] Dou J, Yamagishi H, Zhu Z, Yunus AP, Chen CW. TXT-tool 1.081-6.1 A Comparative Study of the Binary Logistic Regression (BLR) and Artificial Neural Network (ANN) Models for GIS-Based Spatial Predicting Landslides at a Regional Scale. Landslide Dynamics: ISDR-ICL Landslide Interactive Teaching Tools: Springer; 2018:139-51.
[37] Hong H, Naghibi SA, Pourghasemi HR, Pradhan B. GIS-based landslide spatial modeling in Ganzhou City, China. Arabian Journal of Geosciences 2016;9:112.
[38] Pradhan B, Lee S. Landslide susceptibility assessment and factor effect analysis: backpropagation artificial neural networks and their comparison with frequency ratio and bivariate logistic regression modelling. Environmental Modelling & Software 2010;25:747-59.
[39] Park S, Choi C, Kim B, Kim J. Landslide susceptibility mapping using frequency ratio, analytic hierarchy process, logistic regression, and artificial neural network methods at the Inje area, Korea. Environmental earth sciences 2013;68:1443-64.
[40] Glaçon G, Rouvier H. Précisions lithologiques et stratigraphiques sur le "Numidien" de Kroumirie (Tunisie septentrionale). Bull Soc géol France 1967;9:410-7.
[41] Bagga O, Abdeljaouad D, Mercier E. La «zone des nappes» de Tunisie: une marge méso-cénozoïque en blocs basculés

modérément inversée (région de Taberka/Jendouba; Tunisie nord-occidentale). Bulletin Société Géologique de France 2006;177:145-54.
[42] Marzougui W, Melki F, Arfaoui M, Houla Y, Zargouni F. Major faults, salt structures and paleo-ridge at tectonic nodes in Northern Tunisia: contribution of tectonics and gravity analysis. Arabian Journal of Geosciences 2015;8:7601-17.
[43] Belayouni H, Guerrera F, Martín MM, Serrano F. Stratigraphic update of the Cenozoic Sub-Numidian formations of the Tunisian Tell (North Africa): Tectonic/sedimentary evolution and correlations along the Maghrebian Chain. Journal of African Earth Sciences 2012;64:48-64.
[44] Rouvier H. Géologie de l'Extrême Nord-Tunisien [thesis]: Paris. France, Université Pierre et Marie Curie 1977.
[45] Luján M, Storti F, Balanyá J-C, Crespo-Blanc A, Rossetti F. Role of décollement material with different rheological properties in the structure of the Aljibe thrust imbricate (Flysch Trough, Gibraltar Arc): an analogue modelling approach. Journal of Structural Geology 2003;25:867-82.
[46] Attewell P, Farmer I, Glossop N. Ground deformation caused by tunnelling in a silty alluvial clay. Ground Engineering 1978;11.
[47] NIM. http://www.meteo.tn/htmlen/accueil.php.
[48] Van Westen CJ, Castellanos E, Kuriakose SL. Spatial data for landslide susceptibility, hazard, and vulnerability assessment: an overview. Engineering geology 2008;102:112-31.
[49] Corominas J, van Westen C, Frattini P, et al. Recommendations for the quantitative analysis of landslide risk. Bulletin of engineering geology and the environment 2014;73:209-63.
[50] Mohammady M, Pourghasemi HR, Pradhan B. Landslide susceptibility mapping at Golestan Province, Iran: a comparison between frequency ratio, Dempster–Shafer, and weights-of-evidence models. Journal of Asian Earth Sciences 2012;61:221-36.
[51] Park N-W. Application of Dempster-Shafer theory of evidence to GIS-based landslide susceptibility analysis. Environmental Earth Sciences 2011;62:367-76.
[52] Yalcin A, Reis S, Aydinoglu A, Yomralioglu T. A GIS-based comparative study of frequency ratio, analytical hierarchy process, bivariate statistics and logistics regression methods for landslide susceptibility mapping in Trabzon, NE Turkey. Catena 2011;85:274-87.
[53] Gruber S, Haeberli W. Permafrost in steep bedrock slopes and its temperature-related destabilization following climate change. Journal of Geophysical Research: Earth Surface 2007;112.
[54] Rozos D, Pyrgiotis L, Skias S, Tsagaratos P. An implementation of rock engineering system for ranking the instability potential of natural slopes in Greek territory. An application in Karditsa County. Landslides 2008;5:261-70.
[55] Pourghasemi HR, Pradhan B, Gokceoglu C. Application of fuzzy logic and analytical hierarchy process (AHP) to landslide susceptibility mapping at Haraz watershed, Iran. Natural hazards 2012;63:965-96.
[56] Süzen ML, Doyuran V. Data driven bivariate landslide susceptibility assessment using geographical information systems: a method and application to Asarsuyu catchment, Turkey. Engineering Geology 2004;71:303-21.
[57] Komac M. A landslide susceptibility model using the analytical hierarchy process method and multivariate statistics in perialpine Slovenia. Geomorphology 2006;74:17-28.
[58] Nefeslioglu HA, Duman TY, Durmaz S. Landslide susceptibility mapping for a part of tectonic Kelkit Valley (Eastern Black Sea region of Turkey). Geomorphology 2008;94:401-18.
[59] Yilmaz C, Topal T, Süzen ML. GIS-based landslide susceptibility mapping using bivariate statistical analysis in Devrek (Zonguldak-Turkey). Environmental earth sciences 2012;65:2161-78.
[60] Nagarajan R, Roy A, Kumar RV, Mukherjee A, Khire M. Landslide hazard susceptibility mapping based on terrain and climatic factors for tropical monsoon regions. Bulletin of Engineering Geology and the Environment 2000;58:275-87.
[61] Demir G, Aytekin M, Akgün A, Ikizler SB, Tatar O. A comparison of landslide susceptibility mapping of the eastern part of the North Anatolian Fault Zone (Turkey) by likelihood-frequency ratio and analytic hierarchy process methods. Natural hazards 2013;65:1481-506.
[62] Congedo L. Semi-automatic classification plugin documentation. Release 2016;4:29.
[63] RCADJ. http://www.agriculture.tn/?page_id=648.
[64] Eker R, Aydın A. Evaluation of forest roads conditions in terms of landslide susceptibility in Gölyaka and Kardüz Forest Districts (Düzce-Turkey). Eur J Forest Eng 2016;2:54-60.
[65] NOM. http://www.onm.nat.tn/en/index.php.
[66] Dai F, Lee C, Li J, Xu Z. Assessment of landslide susceptibility on the natural terrain of Lantau Island, Hong Kong. Environmental Geology 2001;40:381-91.
[67] Varnes DJ. Landslide hazard zonation: a review of principles and practice1984.
[68] Hong H, Pradhan B, Bui DT, Xu C, Youssef AM, Chen W. Comparison of four kernel functions used in support vector machines for landslide susceptibility mapping: a case study at Suichuan area (China). Geomatics, Natural Hazards and Risk 2017;8:544-69.
[69] Yalcin A. The effects of clay on landslides: A case study. Applied Clay Science 2007;38:77-85.
[70] Hadji R, errahmane Boumazbeur A, Limani Y, Baghem M, el Madjid Chouabi A, Demdoum A. Geologic, topographic and climatic controls in landslide hazard assessment using GIS modeling: a case study of Souk Ahras region, NE Algeria. Quaternary International 2013;302:224-37.
[71] Hadji R, Limani Y, Demdoum A. Using multivariate approach and GIS applications to predict slope instability hazard case study of Machrouha municipality, NE Algeria. Information and Communication Technologies for Disaster Management (ICT-DM), 2014 1st International Conference on; 2014: IEEE. p. 1-10.
[72] Dempster AP. Upper and lower probabilities induced by a multivalued mapping. The annals of mathematical statistics 1967:325-39.
[73] Shafer G. A mathematical theory of evidence: Princeton university press; 1976.
[74] Lee S, Hwang J, Park I. Application of data-driven evidential belief functions to landslide susceptibility mapping in Jinbu, Korea. Catena 2013;100:15-30.
[75] Bonham-Carter G, Agterberg F, Wright D. Integration of geological datasets for gold exploration in Nova Scotia. Digital Geologic and Geographic Information Systems 1988:15-23.
[76] Van Westen C, Rengers N, Soeters R. Use of geomorphological information in indirect landslide susceptibility assessment. Natural hazards 2003;30:399-419.
[77] Neuhäuser B, Damm B, Terhorst B. GIS-based assessment of landslide susceptibility on the base of the weights-of-evidence

model. Landslides 2012;9:511-28.
[78] Pradhan B, Oh H-J, Buchroithner M. Weights-of-evidence model applied to landslide susceptibility mapping in a tropical hilly area. Geomatics, Natural Hazards and Risk 2010;1:199-223.
[79] Chiu CF, Yan WM, Yuen K-V. Estimation of water retention curve of granular soils from particle-size distribution—a Bayesian probabilistic approach. Canadian Geotechnical Journal 2012;49:1024-35.
[80] Cao Z, Wang Y. Bayesian model comparison and selection of spatial correlation functions for soil parameters. Structural Safety 2014;49:10-7.
[81] Reichenbach P, Rossi M, Malamud B, Mihir M, Guzzetti F. A review of statistically-based landslide susceptibility models. Earth-Science Reviews 2018.
[82] Chung C-JF, Fabbri AG. Probabilistic prediction models for landslide hazard mapping. Photogrammetric engineering and remote sensing 1999;65:1389-99.
[83] Chung C-JF, Fabbri AG. Validation of spatial prediction models for landslide hazard mapping. Natural Hazards 2003;30:451-72.
[84] Yesilnacar E, Topal T. Landslide susceptibility mapping: a comparison of logistic regression and neural networks methods in a medium scale study, Hendek region (Turkey). Engineering Geology 2005;79:251-66.
[85] Hadji R, Rais K, Gadri L, Chouabi A, Hamed Y. Slope Failure Characteristics and Slope Movement Susceptibility Assessment Using GIS in a Medium Scale: A Case Study from Ouled Driss and Machroha Municipalities, Northeast Algeria. Arabian Journal for Science and Engineering 2016:1-20.
[86] Horn H, Deere D. Frictional characteristics of minerals. Geotechnique 1962;12:319-35.